1	Superior CO ₂ /N ₂ Separation Performance of High Branched Poly(1,3 dioxolane) Plasticized
2	by Polyethylene Glycol
3	
4	Wenji Guo, Thien N. Tran, Himangshu Mondal, Skye Schaefer, Liang Huang*,
5	and Haiqing Lin*
6	
7	Department of Chemical and Biological Engineering, University at Buffalo, The State University
8	of New York, Buffalo, NY 14260, USA
9	
10	* Corresponding authors:
11	H. Lin, Email: haiqingl@buffalo.edu
12	L. Huang, Email: huangliang0228@163.com
13	
14	
15	
16	
17	Revised submission to Journal of Membrane Science
18	

Abstract

19

20

21

22

23

24

25

26

27

28

29

30

31

32

33

34

With its high content of CO₂-philic ether oxygen groups, poly(1,3-dioxolane) (PDXLA) has emerged as an attractive platform to achieve excellent CO₂/N₂ separation properties for postcombustion carbon capture. Herein we demonstrate that the separation properties of PDXLA can be further enhanced by plasticizing with miscible polyethylene glycol (PEG)-based additives using an integrated experimentation and modeling approach. The effects of the chain end groups and loading level of the additives on the physical properties of the blends are thoroughly investigated, including glass transition temperature (T_g) , fractional free volume, and gas transport properties, and the effects can be satisfactorily described using models available for homogeneous blends. Notably, a T_g -integrated free volume model is adapted to successfully interpret the unified effect of the blend composition and temperature on gas diffusivity and permeability. A sample containing 45 mass% PEG dimethyl ether (PEGDME with a molecular mass of 240 g/mol) displays stable mixed-gas CO₂ permeability of 1540 Barrer and CO₂/N₂ selectivity of 40 when challenged with a model flue gas at 60 °C, outperforming Robeson's 2008 upper bound. Elucidating how small plasticizers impact gas transport in homogeneous blends may unravel a facile way to design highperformance membranes for gas separations.

35

36

Keywords: poly(1,3-dioxolane); CO_2/N_2 separation membranes; T_g -integrated free volume model;

polyethylene glycol dimethyl ether; plasticizer

38

37

1. Introduction

39

40

41

42

43

44

45

46

47

48

49

50

51

52

53

54

55

56

57

58

59

60

Membrane technology has become a leading approach for CO₂ capture from fossil fuelderived flue gas (or CO₂/N₂ separation) to reduce the CO₂ emissions to the atmosphere because of its inherent advantages, such as great energy efficiency, absence of chemical wastes, low maintenance, and small footprint [1-4]. To realize their practical applications, membrane materials should exhibit high CO₂ permeability and CO₂/N₂ selectivity. Poly(ethylene oxide) (PEO)-based materials have attracted significant interest for CO₂/N₂ separation because of their low glass transition temperature (T_g) (yielding flexible chains and thus high gas diffusivity) and strong affinity towards CO₂ (inducing high solubility selectivity and thus high permeability selectivity) [5, 6], such as cross-linked PEO [7-10] and block copolymers [11-13]. These PEO-based materials can be further dispersed with nanoporous nanoparticles (NPs) to form mixed matrix materials with enhanced CO₂/N₂ separation performance, such as metalorganic frameworks (MOFs) or metal-organic polyhedra (MOPs) with high porosity and gas permeability [2, 14-18]. However, it is still challenging to eliminate the interfacial voids between the polymers and NPs, which tend to decrease gas selectivity [16]. PEO-based materials have also been augmented with miscible small molecules to improve gas permeability, such as liquid polyethylene glycol (PEG) [14, 19-22], PEG dimethyl ether (PEGDME) [17, 23-28], crown ether [29], salts [30], and carboxylic acids [31]. The addition of the small molecules plasticizes the polymers, decreasing the T_g and increasing the CO₂ diffusivity. For instance, adding 60 mass% 18-Crown-6 in a cross-linked PEO decreased T_g from -61 to -74 °C and increased CO₂ permeability from 600 to 1340 Barrer (1 Barrer = 10⁻¹⁰ cm³(STP) cm cm⁻² s⁻¹

cmHg⁻¹) while the CO₂/N₂ selectivity varied from 51 to 48 [29].

We have recently reported highly branched poly(1,3 dioxolane) (PDXLA) with higher contents of ether oxygen groups than PEO and thus superior CO_2/N_2 separation properties to PEO [32-34]. Figure 1a illustrates the synthesis of the macromonomer (DXLA) from 1,3 dioxolane, which is then photopolymerized to form PDXLA (Figure 1c,d). The repeating units in the DXLA can be varied from 5 to 16, and the obtained polymers are amorphous. Increasing the repeating unit number (n) increases gas permeability before leveling off at n = 8 [33]. Therefore, DXLA with n = 8 is selected for this study.

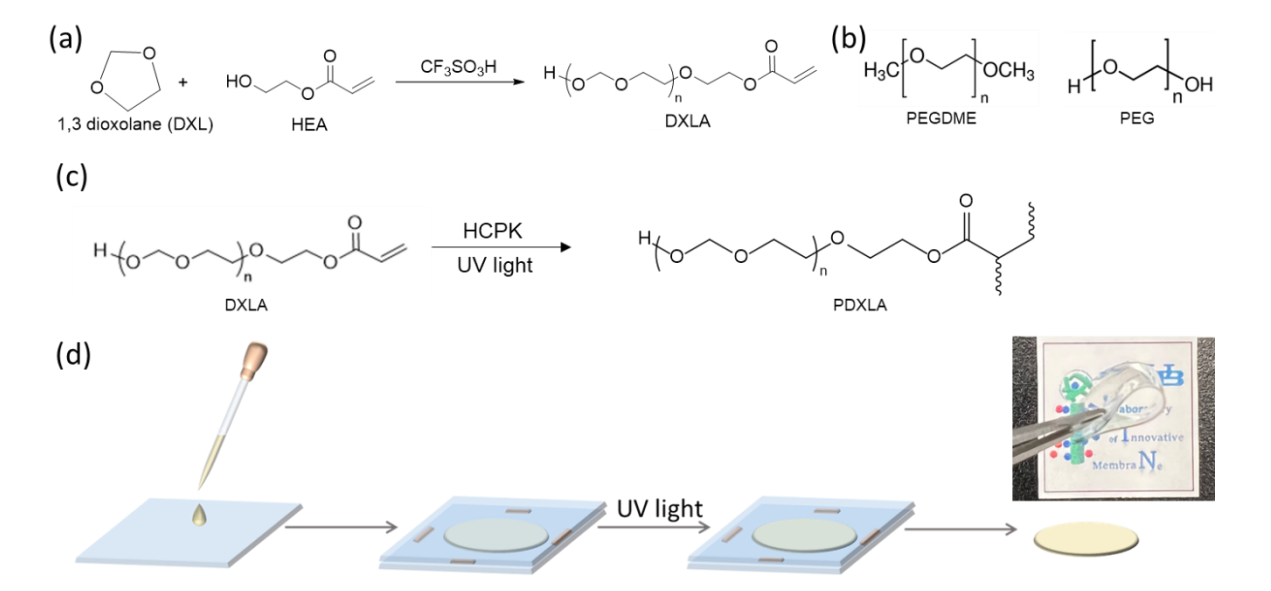


Figure 1. (a) Procedures to synthesize DXLA. (b) Chemical structures of PEGDME and PEG. (c) Photopolymerization of DXLA to form PDXLA. (d) Schematic of the preparation of PDXLA films with a photo of a DME240-45 film. More photos of the films are shown in Figure S1.

Herein we demonstrate that PDXLA can be plasticized with liquid additives to form homogeneous blends with improved CO₂/N₂ separation performance. Specifically, three PEGs with similar chemical structures are investigated, including PEG with molecular mass (Mn) of 400 g/mol (PEG400) and PEGDME with Mn of 240 and 500 g/mol (denoted as PEGDME240 and PEGDME500, respectively). The physical properties and pure-gas separation properties of these

blends were thoroughly characterized. The effect of the additive content on gas diffusivity and permeability can be satisfactorily described using a T_g -integrated free volume model, which has a form similar to Vogel-Tammann-Fulcher (VTF) equation used to describe ion transport. PEGDME240 is the most effective to improve gas permeability among the three additives studied. The sample containing 45 mass% PEGDME240 (DME240-45) renders the best CO_2/N_2 separation properties. When evaluated with model flue gas, it exhibits robust separation properties above Robeson's 2008 upper bound.

2. Experimental

2.1. Materials

1,3-Dioxolane (DXL), 1-hydroxycyclohexyl phenyl ketone (HCPK), PEGDME500, and PEG400 were purchased from Sigma-Aldrich Corporation (St. Louis, MO). 2-Hydroxyethyl acrylate (HEA) and triflic acid (TfOH) were obtained from Acros Organics (Fair Lawn, NJ). PEGDME240 was procured from TCI Chemical Trading Co. (Chuo-ku, Tokyo, JP). Dichloromethane (DCM) was acquired from Fisher Scientific (Hampton, NH) and dried with 3A molecular sieves (Acros Organics) before use. CO₂, He, and N₂ (99.9%) were supplied by Airgas, Inc. (Radnor, PA), and C₂H₆ (99.9%) was purchased from Jackson Welding and Gas Products (Rochester, NY).

2.2. Synthesis of DXLA and PDXLA-based polymers

DXLA was synthesized by cationic ring-opening polymerization of DXL following the procedures described in our previous work (cf. Figure 1a) [32, 33]. TfOH and HEA were used as an initiator and a co-initiator (or chain transfer reagent), respectively. The molar ratio of DXL to HEA was controlled at 8.0 to obtain DXLA with a repeating unit of \approx 8. To fabricate PDXLA-

based blends, the DXLA was mixed with HCPK (0.1 mass%) and the desired amount of the additive (*i.e.*, PEGDME or PEG). The solution was formed into thin films with a controlled thickness (≈ 250 μm) before photopolymerization using 254-nm UV light and procedures described elsewhere [9]. The samples containing PEGDME240, PEGDME500, and PEG400 are denoted as DME240-xx, DME500-xx, or PEG400-xx, respectively, where xx represents the mass percentage of the additive in the blends.

2.3. Characterization of DXLA and the PDXLA-based polymers

A Varian Inova 500 MHz NMR spectrometer was used to characterize the DXLA samples. A Fourier transform infrared (FTIR) spectrometer (Vertex 70 Bruker, Billerica, MA) with attenuated total reflection (ATR) was employed. Differential Scanning Calorimetry (DSC, Q2000, TA Instruments, New Castle, DE) was used to determine thermal transitions. The polymers were heated from -90 °C to 80 °C at 10 °C min⁻¹ before quenching in the N₂ atmosphere for three cycles, and the third heating cycle was used to derive the properties. The density of the films was determined using Mettler Toledo XS64 analytical balance with a density measurement kit [29, 33]. Decane was used as the auxiliary liquid because it is non-ploar and has very low sorption in the polar PDXLA-based films. The initial mass readings in decane were used for calculation to further avoid the interference by the decane sorption in the films. For each sample, more than three films were measured, and the average density value is reported with the standard deviation.

2.4. Determination of gas transport properties

Constant-volume and variable-pressure apparatus were employed to determine pure-gas permeability (P_A) at temperatures (T) ranging from 23 to 60 °C [32]. The leak rate of the system $[(dp_{I,A}/dt)_{leak}, cmHg/s]$ was measured at the beginning of the permeation test, and the steady-state

pressure increasing rate in the downstream volume $[(dp_{I,A}/dt)_{ss}, cmHg/s]$ was recorded after the feed pressure $(p_{2,A}, bar)$ was applied. The P_A was calculated using Equation 1:

$$P_{A} = \frac{V_{d}l}{p_{2,A}ART} \left[\left(\frac{dp_{1,A}}{dt} \right)_{SS} - \left(\frac{dp_{1,A}}{dt} \right)_{leak} \right] \tag{1}$$

- where V_d is the downstream volume (cm³), l is the film thickness (cm), A is the film area (cm²), and R is the gas constant.
- Constant-pressure and variable-volume apparatus were employed to determine mixed-gas permeability using a gas mixture containing was 20% CO₂ and 80% N₂ [29, 32]. Helium with a flow rate of S was used to sweep the permeated gas to a Micro GC for analysis (Inficon Inc., Syracuse, NY). Mixed-gas permeability was calculated using Equation 2:

134
$$P_A = \frac{x_A Sl}{x_{He} A(p_{2,A} - p_{1,A})} \tag{2}$$

- where x_A and x_{He} refer to the molar fraction of gas A and helium in the sweep-out stream, respectively.
- Dual-volume and dual-transducer apparatus were used to determine gas sorption isotherms in the polymers based on a pressure decay method [33]. The sample (3-4 g) was kept in a sample cell. When a known amount of the gas was introduced to the cell, the pressure decreased, and the pressure change can be used to calculate the gas sorption by the samples (C_A , cm³(STP) atm⁻¹). Gas solubility coefficient (S_A) at the equilibrium pressure (p_A , atm) is calculated using Equation 3:

$$S_A = C_A/p_A \tag{3}$$

Gas diffusivity coefficient (D_A , cm² s⁻¹) in polymers is usually calculated using Equation 4 [3]:

$$D_A = P_A / S_A \tag{4}$$

3. Results and discussion

145

146

147

3.1. Physical properties of the PDXLA-based blends

Figure 2a shows the ¹H NMR spectrum of DXLA and the assignment of the chemical shifts for the protons. The *n* value of DXLA is the ratio of the resonance intensities of protons from DXL units (chemical shifts at 3.73 and 4.73 ppm) to those of α -acryloyl protons (chemical shifts at 5.82, 6.13, and 6.42 ppm). The *n* value for the synthesized DXLA is \approx 8, consistent with the ratio of the monomer (DXL) to the initiator (HEA).

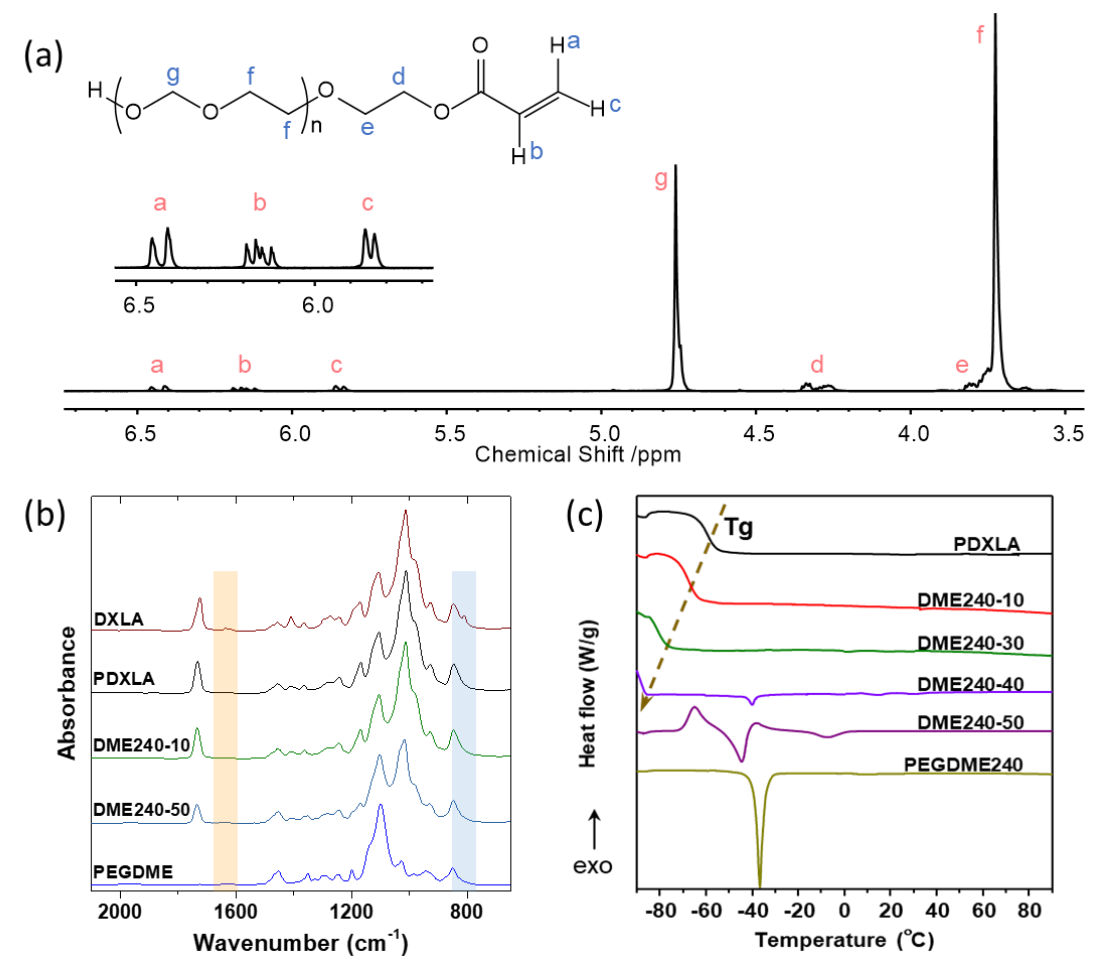


Figure 2. Chemical structure and physical properties of DXLA and the PDXLA-based blends. (a) ¹H NMR spectrum of DXLA. (b) FTIR spectra of DXLA and DME240-xx. An enlarged image of the shadowed region is shown in Figure S2. (c) Comparison of DSC curves for the DME240-xx.

Figures 2b and S2 compare the FTIR spectra of the representative prepolymer solutions before and after the photopolymerization, such as DXLA and PDXLA. As shown in Figures 2b

and S2, the C=C absorption peaks (810 and 1650 cm⁻¹) in DXLA disappear after the polymerization, suggesting the entire conversion of the DXLA [29, 33]. Additionally, as the PEGDME content increases in the blends, the absorption peaks of the C-O-C stretching (1000 cm⁻¹) and C=O stretching (1740 cm⁻¹) in PDXLA decrease. Figure S3 compares the FTIR spectra of the additives, PDXLA, and their blends. PEGDME240 and PEGDME500 exhibit almost the same spectra because of their similar chemical structures. PDXLA displays a peak at 3508 cm⁻¹ for the O-H stretching, which red-shifts to 3485 cm⁻¹ in PEG400-40, indicating the formation of the hydrogen bonding between PEG400 and PDXLA.

Figures 1d and S1 displays the photos of example films of PDXLA and DME240-45. Both films are flexible and mechanically strong for handling. Figure 2c presents the DSC curves of DME240-xx samples. The blends containing PEGDME240 higher than 40 mass% show a melting peak of \approx 10 °C, indicating that the additive induces the polymer crystallization. Nevertheless, all samples are amorphous at 23 °C or above. Figure 3a shows that increasing the PEGDME240 content in the blends decreases the T_g because of the plasticization effect. The T_g for the blends containing more than 40% PEGDME240 cannot be observed because the T_g is lower than the testing limit of our equipment (*i.e.*, -90 °C). The DSC curves for other blends are displayed in Figure S4a.

The T_g of homogeneous blends can be described using Fox Equation [29, 35, 36]:

$${}^{1}/T_{g} = {}^{W_{1}}/T_{g,1} + {}^{W_{2}}/T_{g,2}$$
 (5)

where w is the mass percentage, and the subscripts of 1 and 2 refer to the polymer (PDXLA) and additive, respectively.

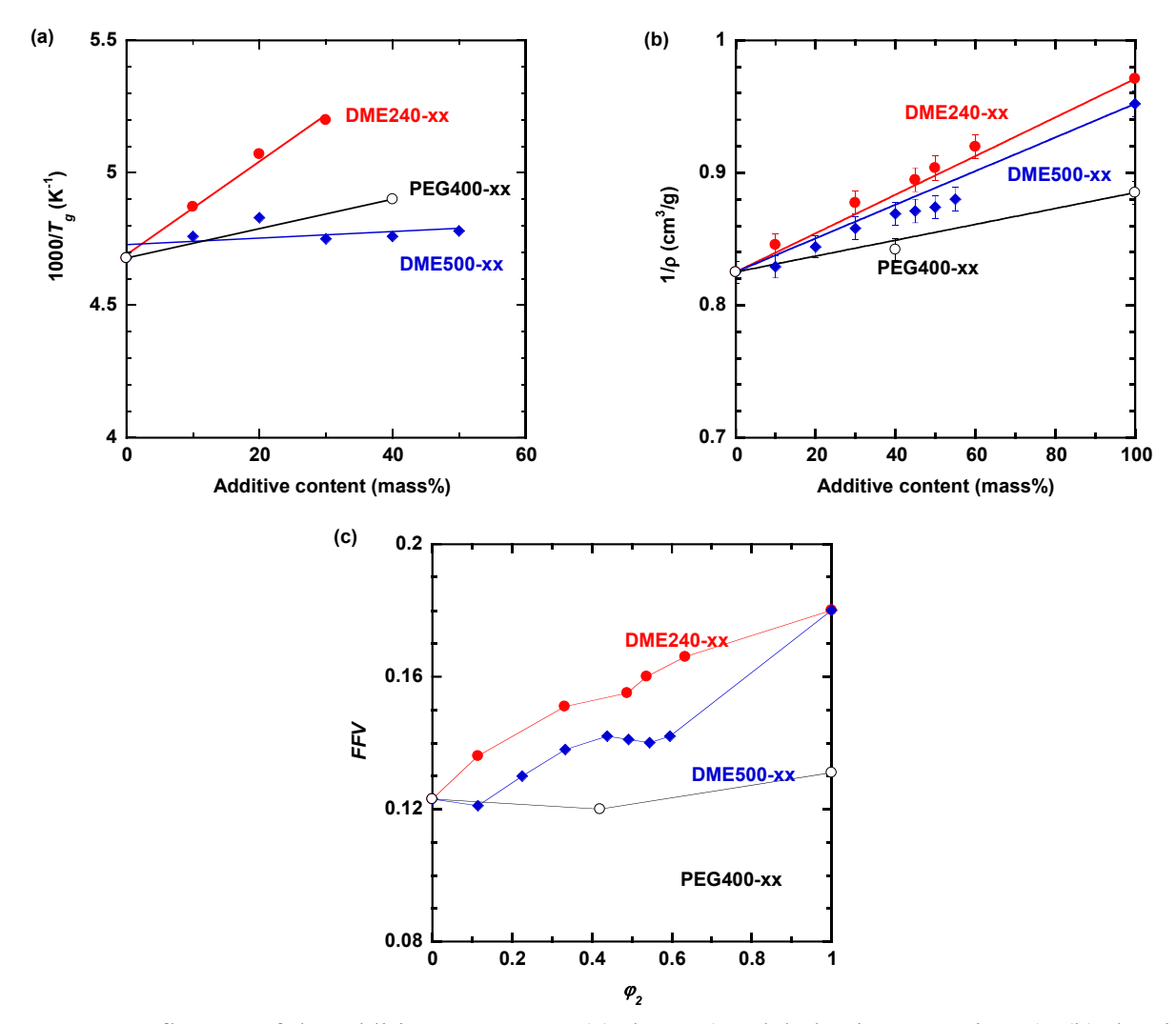


Figure 3. Influence of the additive content on (a) the T_g (modeled using Equation 5), (b) density (modeled using Equation 6), and (c) FFV. The detailed values are summarized in Tables 1 and S1.

Figure 3a displays that the T_g of the blends can be satisfactorily described using Equation 5 with the $T_{g,2}$ value of -120 °C for PEGDME240, -67 °C for PEGDME500, and -82 °C for PEG400, lower than the $T_{g,1}$ of -59 °C. The successful modeling also confirms that the additives are miscible with PDXLA. PEGDME240 exhibits lower T_g than PEGDME500 and PEG400 because of the lower molecular weight and the lack of hydrogen bonding. Moreover, the equation predicts the T_g value of -88, -92, and -95 °C for DME240-40, DME240-45, and DME240-50, respectively, confirming that their T_g 's are too low to detect using our apparatus.

Table 1. Physical properties of DME240-xx samples, including φ_2 , ρ , T_g , FFV, ether oxygen content, and CO_2/N_2 separation properties at 3.0 bar.

Samples	φ_2	ρ (g/cm³)	<i>T_g</i> (°C)	FFV	Oxygen content (mol/L)	Permeability (Barrer)		CO ₂ /N ₂
1						CO_2	N_2	selectivity
PDXLA	0	1.212±0.005	-59	0.123	29.1	220	4.0	56
DME240-10	0.12	1.183 ± 0.008	-68	0.136	28.2	380	7.4	51
DME240-30	0.33	1.140 ± 0.005	-81	0.151	26.9	830	17	48
DME240-45	0.49	1.118 ± 0.003	-88*	0.155	26.1	1400	32	45
DME240-50	0.54	1.107 ± 0.008	-92*	0.160	25.8	1700	40	42
PEG400-40	0.42	1.188 ± 0.009	-69	0.120	26.2	360	6.5	56

^{*} Estimated using Equation 5.

Figure 3b illustrates the impact of the additive loading on the density (ρ). Increasing the loading decreases the density, and PEGDME240 is most effective in lowering the density among the three additives, consistent with its lowest T_g . The ρ can be described using the additive model, as shown below [16]:

$$\frac{1}{\rho} = \frac{w_1}{\rho_1} + \frac{w_2}{\rho_2} \tag{6}$$

The fitting is satisfactory and does not require any adjustable parameters. The ρ_2 values are provided by the manufacturers and recorded in Tables 1 and S1. The volume fraction of the additive (φ_2) can then be estimated using Equation 7:

$$\varphi_2 = \frac{w_2 \rho}{\rho_2} \tag{7}$$

The φ_2 values are also recorded in Tables 1 and S1.

The density can be used to derive fractional free volume (*FFV*), an important parameter influencing gas diffusivity, using Equation 8 [37]:

$$FFV = \frac{V - V_0}{V} = \frac{V - 1.3V_W}{V} \tag{8}$$

where V is the specific volume of the polymer, V_0 is the specific occupied volume at 0 K, and V_w is the Van der Waals volume estimated using the group contribution method. The parameters are recorded in Table S2. Figure 3c shows that the FFV increases with the increasing φ_2 because the additives act as a plasticizer. The PEG400-xx have the lowest FFV because the hydrogen bonding between PEG400 and PDXLA (cf. Figure S3) improves the efficiency of the chain packing. The introduction of the PEGDME240 leads to the highest FFV among the three additives, consistent with its lowest T_g and density.

3.2. Pure-gas CO₂/N₂ separation properties

Figure 4a,b exhibits the influence of the φ_2 on pure-gas CO₂ permeability and CO₂/N₂ selectivity of the blends at 35 °C, respectively. Increasing the additive concentration increases gas permeability with a slight decrease in CO₂/N₂ selectivity. At the same loading level, gas permeability decreases in the order of DME240-xx, DME500-xx, and PEG400-xx, consistent with the order of decreasing FFV and increasing T_g . The films are also stable after the high-pressure permeation tests. For example, PDXLA has a thickness of $208 \pm 6 \mu m$ before the test and $207 \pm 7 \mu m$ after the test, while DME240-45 has a thickness of $187 \pm 6 \mu m$ before the test and $183 \pm 7 \mu m$ after the test despite its high content of PEGDME240.

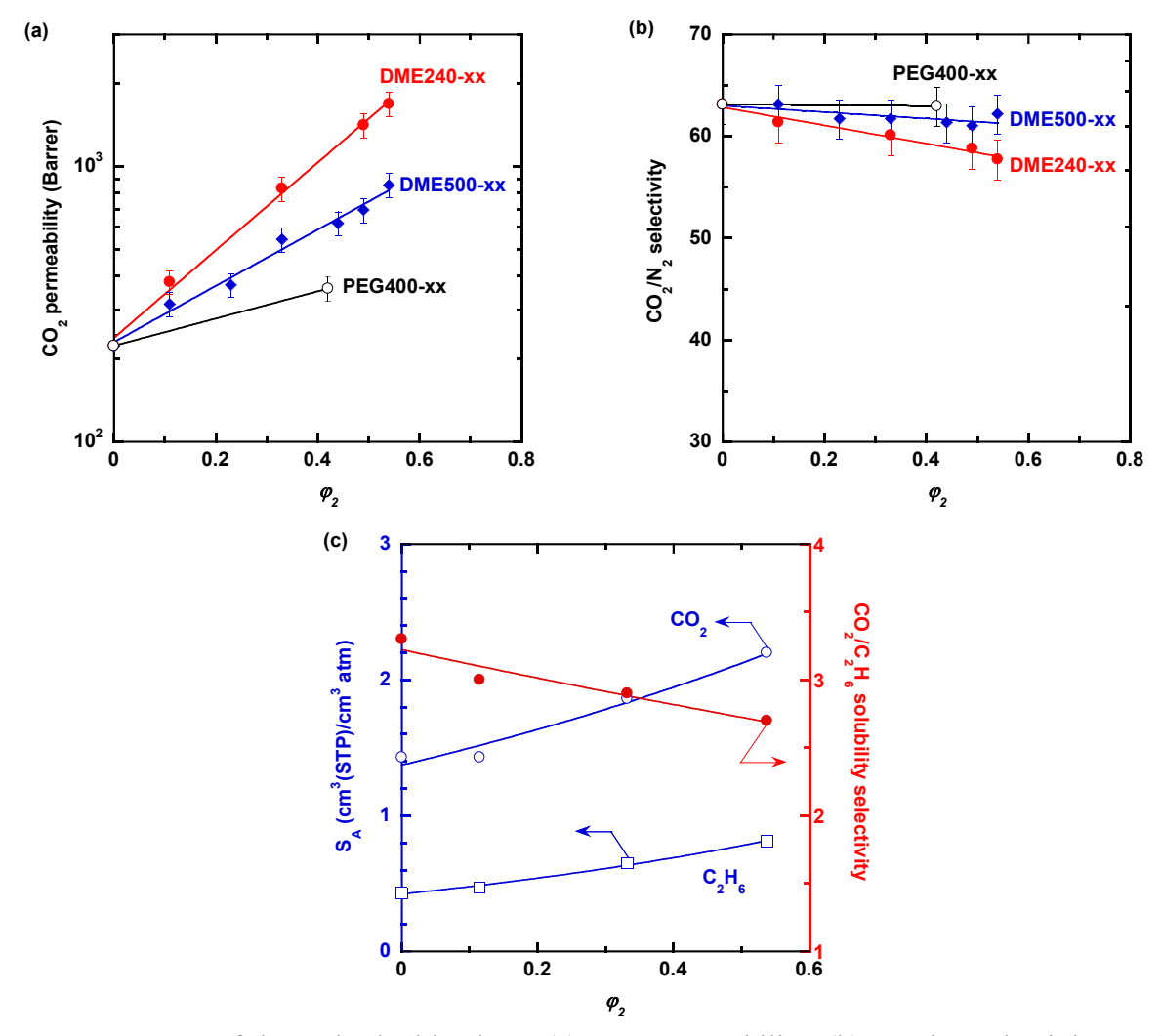


Figure 4. Impact of the φ_2 in the blends on (a) CO₂ permeability, (b) CO₂/N₂ selectivity, and (c) CO₂ and C₂H₆ solubility coefficient and CO₂/C₂H₆ solubility selectivity at 35 °C (cf. Table S3). The curves are the best fits of Equation 9.

Gas transport properties of homogenous blends can be described by the following equations [9, 38]:

$$ln\gamma = \varphi_1 ln\gamma_1 + \varphi_2 ln\gamma_2 \tag{9}$$

where γ_A can be P_A , S_A , D_A , or their selectivities. As shown in Figure 4a,b, the data for all additives can be fitted satisfactorily. PEGDME500 is estimated to have CO₂ permeability of 2300 Barrer and CO₂/N₂ selectivity of 45, consistent with the literature [20, 39]. By contrast, PEGDME240 is

estimated to exhibit CO₂ permeability of 9600 Barrer, more than 40 times that of PDXLA, and a moderate CO₂/N₂ selectivity of 35.

To elucidate the impact of the additive loading on the gas transport properties, the gas sorption isotherms in DME240-xx at 35°C were determined, as they present the most attractive separation properties. Figure 4c shows the increase of CO₂ solubility with the increasing PEGDME240 loading because of the increased *FFV*, though it is counteracted by the decreased content of the CO₂-philic ether oxygen groups (cf. Figure S4b). For example, DME240-50 exhibits CO₂ solubility of 2.2 cm³(STP) cm⁻³ atm⁻¹, higher than that of PDXLA (1.4 cm³(STP) cm⁻³ atm⁻¹), though DME240-50 shows an ether oxygen content of 25.8 mol/L compared with 29.1 mol/L for PDXLA.

C₂H₆ is chosen as a marker for N₂ because N₂ solubility is too low to determine using our apparatus. C₂H₆ does not have specific interactions with the ether oxygen groups (similar to N₂), and thus CO₂/N₂ selectivity is expected to follow a trend similar to CO₂/C₂H₆ solubility selectivity [32]. Figure 4c displays that increasing the loading of PEGDME240 increases the C₂H₆ solubility because of the increased *FFV*, which can also be described using Equation 9 [38]. Nevertheless, the CO₂/C₂H₆ solubility selectivity slightly decreases from 3.3 for PDXLA to 2.7 for DME240-50, which can be ascribed to the decreased content of the CO₂-philic ether oxygen content.

3.3. Modeling of gas transport properties using the T_g -integrated free volume model

CO₂ diffusivity increases with increasing PEGDME240 loading, consistent with the decreased T_g . For instance, increasing the PEGDME240 loading from 0 to 50 mass% increases the CO₂ diffusivity from 1.2×10^{-6} to 5.8×10^{-6} cm²/s (Table S3). Gas diffusivity in polymers can be described using the free volume model [36, 37, 40]:

$$D_A = D_{A,0} exp\left(-\frac{B_A}{FFV}\right) \tag{10}$$

where $D_{A,0}$ and B_A are adjustable parameters. Figure 5a demonstrates that the CO₂ diffusivity can be satisfactorily described using the free volume model.



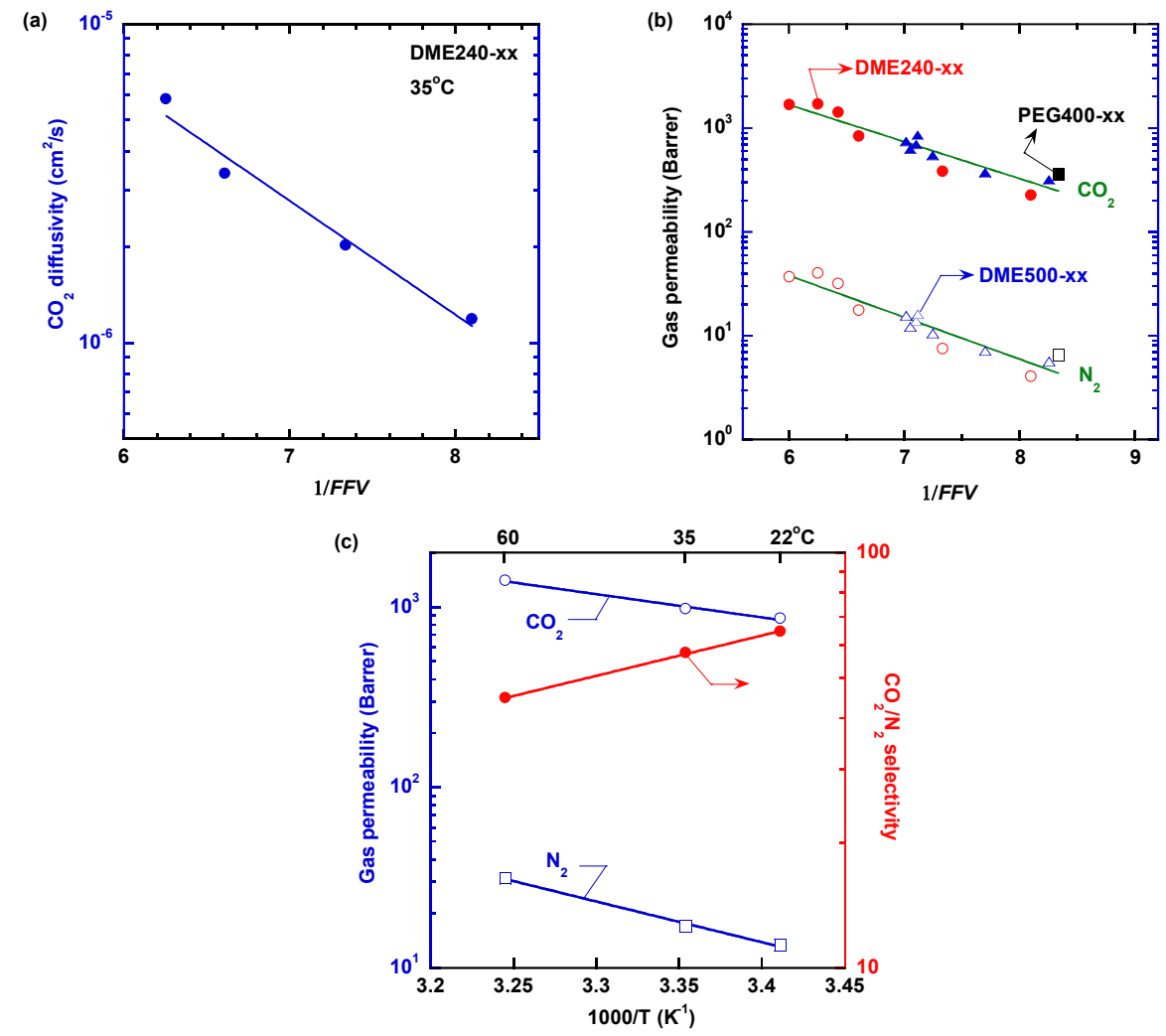


Figure 5. (a) Correlation between the FFV and CO_2 diffusivity using Equation 10 in DME240-xx at 35 °C. (b) Correlation between the FFV and N_2 and CO_2 permeability by Equation 11 for DME240-xx, DME500-xx, and PEG400-xx at 35 °C. (c) Correlation of T and CO_2/N_2 separation properties in DME240-45 using Equation 12.

If the FFV has much more influence on D_A than S_A , Equation 10 can be written as:

$$P_A = S_A D_{A,0} exp\left(-\frac{B_A}{FFV}\right) \tag{11}$$

This assumption is valid for the DME240-xx. For example, increasing the PEGDME240 loading from 0 to 50 mass% increases the CO₂ solubility by 57% and CO₂ diffusivity by 320%. Figure 5b demonstrates that Equation 11 can be satisfactorily used to describe N₂ and CO₂ permeability in the PDXLA-based blends with three additives, confirming that the change in gas permeability can be ascribed to the change in the free volume.

DME240-45 was investigated for gas separation at various temperatures. Figure 5c depicts that increasing the temperature increases gas permeability and decreases gas selectivity, which can be described by the Arrhenius Equation:

$$P_A = P_{A,0} exp\left(\frac{-E_{P,A}}{RT}\right) \tag{12}$$

where $P_{A,0}$ is the front factor (Barrer), and $E_{P,A}$ is the activation energy of permeation (kJ/mol).

The fitting yields the $E_{P,A}$ value of 16 kJ/mol for CO₂ and 30 kJ/mol for N₂, consistent with the greater condensability and smaller kinetic diameter of CO₂ than N₂.

For rubbery polymers, *FFV* can be estimated using Equation 13 [29, 37, 41]:

$$FFV = FFV(T_q) + \alpha_r(T - T_q)$$
(13)

where $FFV(T_g)$ is the apparent FFV at T_g , and α_r is the expansion coefficient of the polymer. Figure 6a presents that the FFV of the PDXLA-based samples can be correlated with the T_g with the $FFV(T_g)$ of 0.042 and α_r of 9.0 × 10⁻⁴ K⁻¹, which are remarkably consistent with those proposed in the literature (0.025 for $FFV(T_g)$ and 7.8 × 10⁻⁴ K⁻¹ for α_r of PEO-based materials) [37].

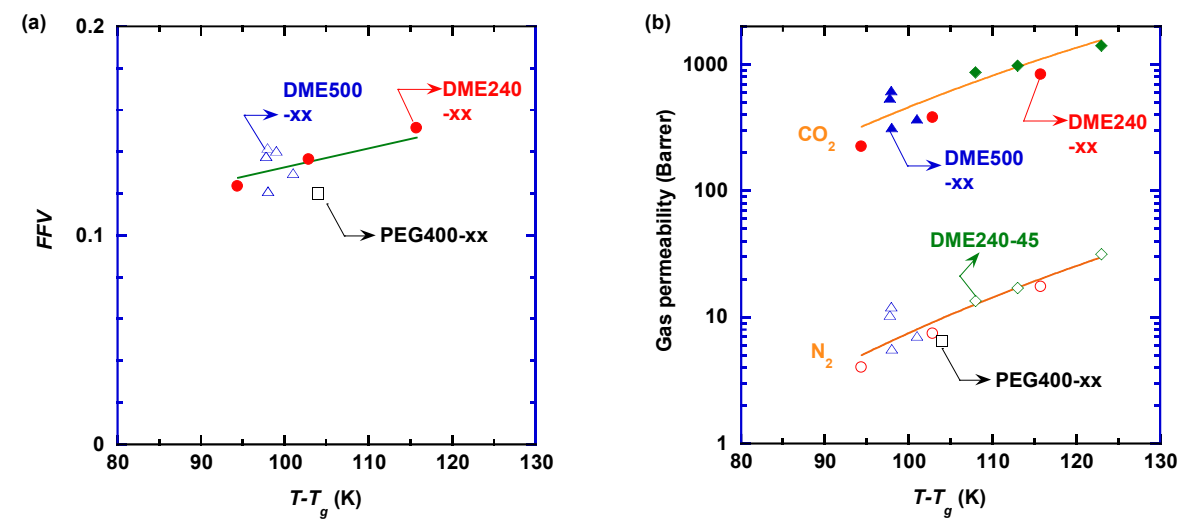


Figure 6. (a) Correlation between the FFV and T_g for the PDXLA-based polymers using Equation 13. (b) Correlation of N_2 (open symbols) and CO_2 (filled symbols) permeability with T_g using the T_g -integrated free volume model (Equation 14) for the PDXLA-based blends and DME240-45 at 20, 25, and 35 °C (green symbols).

Combining Equations 11 and 13 yields [29, 37, 41]:

$$P_A = S_A D_{A,0} exp\left(\frac{-B_A/\alpha_r}{FFV(T_g)/\alpha_r + (T - T_g)}\right)$$
(14)

This equation is similar to the VTF equation used to describe the ion transport and the Williams-Landel-Ferry (WLF) equation to model the viscosity of rubbery polymers. The $FFV(T_g)/\alpha_r$ often has a value of 50 K [42], and the B_A/α_r is related to the activation energy for diffusion (*i.e.*, $E_{D,A}/R = B_A/\alpha_r$). Equation 14 has been used to interpret gas permeability in PEO-based copolymers, but not the blends of PDXLA with liquid plasticizers. Figure 6b shows that the N_2 and CO_2 permeability can be well correlated with (T- T_g), which is impressive considering that the data include permeability for DME240-xx, DME500-xx, and PEG400-xx at 35 °C and DME240-45 at 20, 25, and 35 °C.

3.4. Superior CO₂/N₂ separation performance in DME240-45

The DME240-45 was further evaluated with model flue gas containing CO₂/N₂ of 20/80 at 7.9 bar and 60 °C. Figure 7a displays that the DME240-45 exhibits mixed-gas CO₂ permeability

of 1540 Barrer, N₂ permeability of 39 Barrer, and CO₂/N₂ selectivity of 40. The CO₂/N₂ separation performance is stable during the 20-h test at 60 °C. Nevertheless, a longer-term demonstration of the stability of these blends will be needed for them to be considered for practical applications.



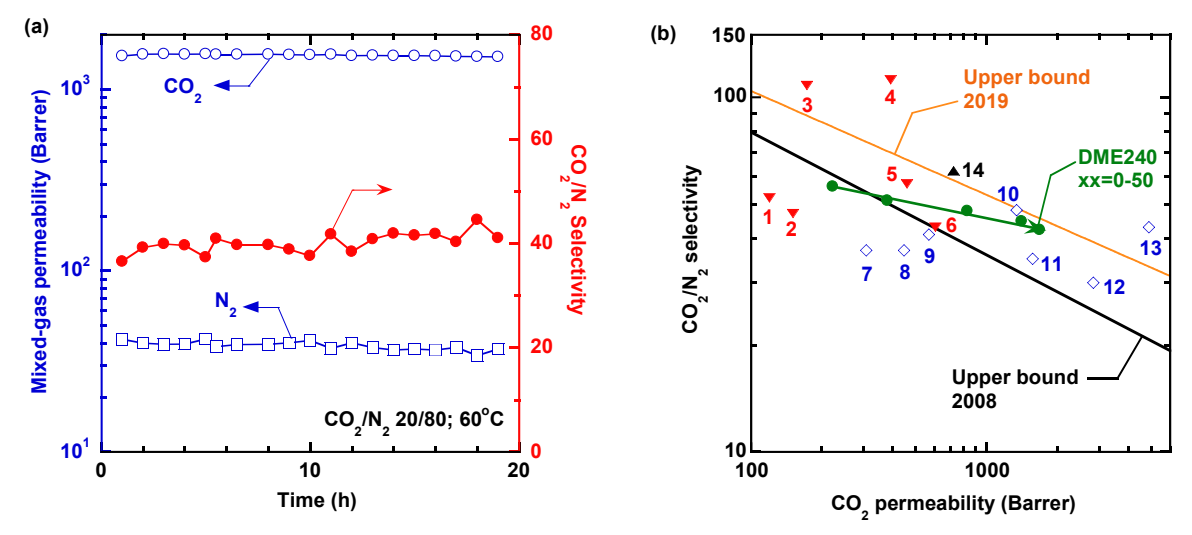


Figure 7. Superior CO₂/N₂ separation properties of DME240. (a) Mixed-gas separation performance of DME240-45 with CO₂/N₂ of 20/80 at 7.9 bar and 60 °C. (b) Comparison of DME240-xx (•) in Robeson's 2008 and 2019 upper bounds with other leading polyethers [43], including Pebax-based blends (\blacktriangledown) [13, 14, 19-21, 44], cross-linked PEO-based blends (\diamondsuit) [9, 17, 23, 24, 27, 29, 39], and PDXLA-*co*-PDXLEA (\blacktriangle) [32]. The details for these polyethers are summarized in Table S4.

Figure 7b compares the CO₂/N₂ separation properties of the DME240-xx with Robeson's 2008 and 2019 upper bounds at 35 °C (*i.e.*, the tradeoff between permeability and selectivity) [43]. The DME240-45 and DME240-50 exhibit CO₂/N₂ separation properties above the 2008 upper bound and close to the 2019 one. Specifically, the DME240-50 shows CO₂ permeability of 1680

Barrer and CO₂/N₂ selectivity of 42, comparable with the leading polyethers in the literature,

including those loaded with PEGDME [17, 24, 27, 39, 44].

4. Conclusion

We demonstrate by experimentation and modeling that PDXLA can be blended with miscible additives (including PEG400, PEGDME240, and PEGDME500) to enhance CO_2 permeability while retaining the high CO_2/N_2 selectivity. Increasing the additive content decreases the density and T_g , which can be satisfactorily described using the additive model and Fox equation, respectively. More importantly, the effect of the additive content and testing temperature on gas permeability and selectivity can be described using a T_g -integrated free volume model. Among the three additives, PEGDME240 renders the most significant impact on the T_g , FFV, and gas permeability because of its lowest T_g and highest FFV and the absence of hydrogen bonding. DME240-45 exhibiting excellent CO_2/N_2 separation properties was further evaluated with model flue gas and demonstrates the separation performance above Robeson's 2008 upper bound, indicating its potential for practical applications. This work lays out a theoretical foundation for a facile and fruitful way to improve gas separation properties by designing thermally stable homogeneous blends.

ACKNOWLEDGMENT

This work was financially supported by the U.S. Department of Energy (DE-FE0031736), the New York State Foundation for Science, Technology, and Innovation (NYSTAR), and the U.S. National Science Foundation (1554236).

REFERENCES

- Y. Han, W. S. Ho. Polymeric membranes for CO₂ separation and capture. J. Membr. Sci. 628 (2021) 119244.
- L. Hu, K. Clark, T. Alebrahim, H. Lin. Mixed matrix membranes for post-combustion carbon capture: From materials design to membrane engineering. J. Membr. Sci. 644 (2022) 120140.

- M. Galizia, W. S. Chi, Z. P. Smith, T. C. Merkel, R. W. Baker, B. D. Freeman. 50th Anniversary perspective: Polymers and mixed matrix membranes for gas and vapor separation: A review and prospective opportunities. Macromolecules. 50 (2017) 7809-7843.
- S. Roussanaly, R. Anantharaman, K. Lindqvist, H. Zhai, E. Rubin. Membrane properties required for post-combustion CO₂ capture at coal-fired power plants. J. Membr. Sci. 511 (2016) 250-264.
- 358 [5] B. Zhu, X. Jiang, S. He, X. Yang, J. Long, Y. Zhang, L. Shao. Rational design of poly(ethylene oxide) based membranes for sustainable CO₂ capture. J. Mater. Chem. A. 8 (2020) 24233-24252.
- J. Liu, X. Hou, H. Park, H. Lin. High-performance polymers for membrane CO₂/N₂ separation. Chem. Eur. J. 22 (2016) 15980-15990.
- C. G. Rodriguez, M. Chwatko, J. Park, C. L. Bentley, B. D. Freeman, N. A. Lynd. Compositionally controlled polyether membranes via mono(mu-alkoxo)bis(alkylaluminum)-Initiated chain-growth network epoxide polymerization: synthesis and transport properties. Macromolecules. 53 (2020) 1191-1198.
- V. A. Kusuma, B. D. Freeman, M. A. Borns, D. S. Kalika. Influence of chemical structure of short chain pendant groups on gas transport properties of cross-linked poly(ethylene oxide) copolymers. J. Membr. Sci. 327 (2009) 195-207.
- H. Lin, E. V. Wagner, J. S. Swinnea, B. D. Freeman, S. J. Pas, A. J. Hill, S. Kalakkunnath,
 D. S. Kalika. Transport and structural characteristics of crosslinked poly(ethylene oxide)
 rubbers. J. Membr. Sci. 276 (2006) 145-161.
- Y. Hirayama, Y. Kase, N. Tanihara, Y. Sumiyama, Y. Kusuki, K. Haraya. Permeation properties to CO₂ and N₂ of poly(ethylene oxide)-containing and crosslinked polymer films. J. Membr. Sci. 160 (1999) 87-99.
- W. Yave, H. Huth, A. Car, C. Schick. Peculiarity of a CO₂-philic block copolymer confined in thin films with constrained thickness: "A super membrane for CO₂-capture". Energy Environ. Sci. 4 (2011) 4656-4661.
- 379 [12] S. R. Reijerkerk, M. H. Knoef, K. Nijmeijer, M. Wessling. Poly(ethylene glycol) and poly(dimethyl siloxane): Combining their advantages into efficient CO₂ gas separation membranes. J. Membr. Sci. 352 (2010) 126-135.
- V. I. Bondar, B. D. Freeman, I. Pinnau. Gas transport properties of poly(ether-*b*-amide) segmented block copolymers. J. Polym. Sci.: Part B: Polym. Phys. 38 (2000) 2051-2062.
- B. Zhang, C. Yang, Y. Zheng, Y. Wu, C. Song, Q. Liu, Z. Wang. Modification of CO₂-selective mixed matrix membranes by a binary composition of poly(ethylene glycol)/NaY zeolite. J. Membr. Sci. 627 (2021) 119239.
- J. Liu, C. R. P. Fulong, L. Hu, L. Huang, G. Zhang, T. R. Cook, H. Lin. Interpenetrating networks of mixed matrix materials comprising metal-organic polyhedra for membrane CO₂ capture. J. Membr. Sci. 606 (2020) 118122.
- L. Hu, J. Liu, L. Zhu, X. Hou, L. Huang, H. Lin, J. Cheng. Highly permeable mixed matrix
 materials comprising ZIF-8 nanoparticles in rubbery amorphous poly(ethylene oxide) for
 CO₂ capture. Sep. Purif. Techn. 205 (2018) 58-65.
- 393 [17] X. Jiang, S. Li, L. Shao. Pushing CO₂-philic membrane performance to the limit by 394 designing semi-interpenetrating networks (SIPN) for sustainable CO₂ separations. Energy 395 Environ. Sci. 10 (2017) 1339-1344.

- J. Shen, G. Liu, K. Huang, W. Jin, K. R. Lee, N. Xu. Membranes with fast and selective gas-transport channels of laminar graphene oxide for efficient CO₂ capture. Angew. Chem. Int. Ed. 127 (2015) 588-592.
- R. He, S. Cong, S. Xu, S. Han, H. Guo, Z. Liang, J. Wang, Y. Zhang. CO₂-philic mixed matrix membranes based on low-molecular-weight polyethylene glycol and porous organic polymers. J. Membr. Sci. 624 (2021) 119081.
- W. Yave, A. Car, K.-V. Peinemann. Nanostructured membrane material designed for carbon dioxide separation. J. Membr. Sci. 350 (2010) 124-129.
- 404 [21] A. Car, C. Stropnik, W. Yave, K.-V. Peinemann. PEG modified poly(amide-b-ethylene oxide) membranes for CO₂ separation. J. Membr. Sci. 307 (2008) 88-95.
- N. P. Patel, R. J. Spontak. Mesoblends of polyether block copolymers with poly(ethylene glycol). Macromolecules. 37 (2004) 1394-1402.
- 408 [23] W. Sun, M. Yin, W. Zhang, S. Li, N. Wang, Q. An. Green techniques for rapid fabrication 409 of unprecedentedly high-performance PEO membranes for CO₂ capture. ACS Sustain. 410 Chem. Eng. 9 (2021) 10167-10175.
- 411 [24] S. Li, X. Jiang, X. Yang, Y. Bai, L. Shao. Nanoporous framework "reservoir" maximizing 412 low-molecular-weight enhancer impregnation into CO₂-philic membranes for highly-413 efficient CO₂ capture. J. Membr. Sci. 570-571 (2019) 278-285.
- J. Cheng, L. Hu, Y. Li, C. Ji, J. Zhou, K. Cen. Improving CO₂ permeability of ceramic hollow fibre-supported composite membranes by blending an ionic liquid in the Pebax/PEGDME selective layer. RSC Adv. 6 (2016) 2055-2064.
- H. Chen, T. S. Chung. CO₂-selective membranes for hydrogen purification and the effect of carbon monoxide (CO) on its gas separation performance. J. Membr. Sci. 37 (2012) 6001-6011.
- 420 [27] S. Quan, S. Li, Z. Wang, X. Yan, Z. Guo, L. Shao. A bio-inspired CO₂-philic network 421 membrane for enhanced sustainable gas separation. J. Mater. Chem. A. 3 (2015) 13758-422 13766.
- W. Yave, A. Car, S. S. Funari, S. P. Nunes, K. V. Peinemann. CO₂-philic polymer membrane with extremely high separation performance. Macromolecules. 43 (2010) 326-333.
- 426 [29] L. Huang, J. Liu, H. Lin. Thermally stable, homogeneous blends of cross-linked 427 poly(ethylene oxide) and crown ethers with enhanced CO₂ permeability. J. Membr. Sci. 428 610 (2020) 118253.
- 429 [30] T. Alebrahim, A. Chakraborty, L. Hu, S. Patil, S. Cheng, D. Acharya, C. M. Doherty, A. J. 430 Hill, T. R. Cook, H. Lin. Gas transport characteristics of supramolecular networks of metal-coordinated highly branched poly(ethylene oxide). J. Membr. Sci. 644 (2022) 120063.
- 432 [31] S. Meshkat, S. Kaliaguine, D. Rodrigue. Enhancing CO₂ separation performance of Pebax® MH-1657 with aromatic carboxylic acids. Sep. Purif. Techn. 212 (2019) 901-912.
- J. Liu, S. Zhang, D. Jiang, C. M. Doherty, A. J. Hill, C. Cheng, H. Park, H. Lin. Highly polar but amorphous polymers with robust membrane CO₂/N₂ separation performance. Joule. 3 (2019) 1881-1894.
- 437 [33] L. Huang, W. Guo, H. Mondal, S. Schaefer, T. N. Tran, H. Lin. Effect of the branch length on structural and CO₂/N₂ separation properties of hyperbranched poly(1,3-dioxolane). 439 Macromolecules. 55 (2022) 382-389.

- J. Liu, G. Zhang, K. Clark, H. Lin. Maximizing ether oxygen content in polymers for membrane CO₂ removal from natural gas. ACS Appl. Mater. Interfaces. 11 (2019) 10933-10940.
- W. Brostow, R. Chiu, I. M. Kalogeras, A. Vassilikou-Dova. Prediction of glass transition temperatures: Binary blends and copolymers. Mater. Lett. 62 (2008) 3152-3155.
- H. Lin, M. Yavari. Upper bound of polymeric membranes for mixed-gas CO₂/CH₄ separations. J. Membr. Sci. 475 (2015) 101-109.
- H. Lin, B. D. Freeman, S. Kalakkunnath, D. S. Kalika. Effect of copolymer composition, temperature, and carbon dioxide fugacity on pure- and mixed-gas permeability in poly(ethylene glycol)-based materials: Free volume interpretation. J. Membr. Sci. 291 (2007) 131-139.
- D. R. Paul. Gas transport in homogeneous multicomponent polymers. J. Membr. Sci. 18 (1984) 75-86.
- 453 [39] Z. Dai, H. Aboukeila, L. Ansaloni, J. Deng, M. Giacinti Baschetti, L. Deng. Nafion/PEG 454 hybrid membrane for CO₂ separation: Effect of PEG on membrane micro-structure and 455 performance. Sep. Purif. Techn. 214 (2019) 67-77.
- J. Park, D. R. Paul. Correlation and prediction of gas permeability in glassy polymer membrane materials via a modified free volume based group contribution method. J. Membr. Sci. 125 (1997) 23-39.
- V. A. Kusuma, J. S. McNally, J. S. Baker, Z. Tong, L. Zhu, C. J. Orme, F. F. Stewart, D.
 P. Hopkinson. Cross-linked polyphosphazene blends as Robust CO₂ separation membranes.
 ACS Appl. Mater. Interfaces. 12 (2020) 30787-30795.
- 462 [42] Y. Karatas, R. D. Banhatti, N. Kaskhedikar, M. Burjanadze, K. Funke, H.-D. Wiemhöfer. Synthesis and modeling of polysiloxane-based salt-in-polymer electrolytes with various additives. J. Phys. Chem. B. 113 (2009) 15473-15484.
- B. Comesaña-Gándara, J. Chen, C. G. Bezzu, M. Carta, I. Rose, M.-C. Ferrari, E. Esposito, A. Fuoco, J. C. Jansen, N. B. McKeown. Redefining the Robeson upper bounds for CO₂/CH₄ and CO₂/N₂ separations using a series of ultrapermeable benzotriptycene-based polymers of intrinsic microporosity. Energy Environ. Sci. 12 (2019) 2733-2740.
- N. Liu, J. Cheng, L. Hu, W. Hou, X. Yang, M. Luo, H. Zhang, B. Ye, J. Zhou. Boosting CO₂ transport of poly(ethylene oxide) membranes by hollow Rubik-like "expressway" channels with anion pillared hybrid ultramicroporous materials. Chem. Eng. J. 427 (2022) 130845.